RSC Advances

PAPER

View Article Online
View Journal | View Issue

Cite this: *RSC Adv.*, 2023, **13**, 27088

Supramolecular Cu(II) nanoparticles supported on a functionalized chitosan containing urea and thiourea bridges as a recoverable nanocatalyst for efficient synthesis of 1*H*-tetrazoles†

Shirin Bondarian, Mohammad G. Dekamin,* Ehsan Valiey and M. Reza Naimi-Jamal

A cost-effective and convenient method for supporting of Cu(II) nanoparticles on a modified chitosan backbone containing urea and thiourea bridges using thiosemicarbazide (TS), pyromellitic dianhydride (PMDA) and toluene-2,4-diisocyanate (TDI) linkers was designed. The prepared supramolecular (CS–TDI–PMDA–TS–Cu(II)) nanocomposite was characterized by using Fourier-transform infrared (FT-IR) spectroscopy, field emission scanning electron microscopy (FESEM), thermogravimetry/differential thermogravimetry analysis (TGA/DTA), energy-dispersive X-ray spectroscopy (EDS), EDS elemental mapping and X-ray diffraction (XRD). The obtained supramolecular CS–TDI–PMDA–TS–Cu(II) nanomaterial was demonstrated to act as a multifunctional nanocatalyst for promoting of multicomponent cascade Knoevenagel condensation/click 1,3-dipolar azide–nitrile cycloaddition reactions very efficiently between aromatic aldehydes, sodium azide and malononitrile under solvent-free conditions and affording the corresponding (*E*)-2-(1*H*-tetrazole-5-yl)-3-arylacrylenenitrile derivatives. Low catalyst loading, working under solvent-free conditions and short reaction time as well as easy preparation and recycling, and reuse of the catalyst for five consecutive cycles without considerable decrease in its catalytic efficiency make it a suitable candidate for the catalytic reactions promoted by Cu species.

Received 26th March 2023
Accepted 16th August 2023

DOI: 10.1039/d3ra01989f

rsc.li/rsc-advances

1. Introduction

Pristine biopolymers and especially their chemically-modified derivatives have been recently found to serve as appropriate leading materials in many research and technology areas including vaccines, medical practice, antibacterial and wound healing dressing, naturally degradable sensors, environmental engineering, buildings, energy storage devices, electrochemistry, food packaging, and replacing conventional petrochemical-based polymers as well as appropriate supports for low-toxic and biodegradable catalytic systems.[1–11] The use of appropriate catalytic systems to prepare important medicinal compounds through environmental-friendly protocols has received significant interest in both academia and industry in recent decades. Two types of catalytic systems are homogeneous and heterogeneous. Homogeneous catalysts are less frequently used in modern industrial and synthetic applications because they suffer from low thermal stability, harsh and prolonged work-up procedures, and waste generation.[12,13] Interestingly, the supramolecular and non-covalent supporting of the homogeneous catalytic species or anchoring of the functional groups on the inorganic or organic supports as well as their hybrid ones to form heterogeneous catalysts can overcome the encountered problems.[8,11,14–25] Various organic or inorganic supports including synthetic polymers, natural polymers such as chitosan and cellulose,[3,4,10,26–28] bentonite,[29,30] SiO_2,[31,32] perlite, graphene oxide,[33,34] MOFs, *etc.* have been used for this purpose.[35–38]

The use of natural polymers, as proper supports, has currently attracted much attention to produce various types of heterogeneous catalysts. Chitosan, among other typical biopolymers, has diverse advantages such as biocompatibility, biodegradability, and non-toxicity. It's surface functional groups including NH_2 and OH, make it an appropriate support for the preparation of heterogeneous catalysts.[9–11,22,25,39–43] Although heterogeneous catalysts usually demonstrate lower catalytic efficiency and selectivity in comparison with homogeneous ones due to their insolubility in the reaction medium, the formation of active catalytic species nanoparticles or the use of nanoscale assemblies of supports may overcome this challenge.[44–48] Indeed, nano-ordered heterogeneous catalytic systems can form a bridge between the gap of homogeneous

Pharmaceutical and Heterocyclic Compounds Research Laboratory, Department of Chemistry, Iran University of Science and Technology, Tehran, 16846-13114, Iran. E-mail: mdekamin@iust.ac.ir

† Electronic supplementary information (ESI) available. See DOI: https://doi.org/10.1039/d3ra01989f

and heterogeneous catalysts through combination of synergistic effects of both systems. The principal goal of nanochemistry and relevant technologies is to follow some useful conditions or chemical reactions for modifying the size, morphology, or surface chemical compositions of the obtained nanomaterials with proper and adjustable chemical activity and selectivity, thermal and mechanical stability, reusability, *etc.*[49] Among them, nanocomposites formed by biopolymeric supports have a spread range of green and environmental friendly beneficial for different applications including catalysts, cosmetic orthodontics, modern construction, electronics, fuel cell, energy storage, *etc.*[50–54] Hence, academia and chemical industry are moving to safer and cleaner strategies of synthesis and manufacturing required chemicals and products by the use of such nanomaterials.[55–61]

Heterogeneous nanocatalysts comprising modified chitosan can be prepared through a variety of chemical modifications such as metal chelation, carboxylation, acylation, sulfation, cyanoethylation, Schiff base formation, *etc.*, owing to the existence of reactive amino and hydroxyl groups.[8,11,62–68] Thus, the modified structures of chitosan are often produced by the chemical manipulation of active sites of OH and NH_2 groups, with the object of improving their efficiency for particular applications. To expand the domain of application in the modified chitosan-based nanomaterials, new derivatives comprising diverse functional groups grafted onto the chitosan backbone are expected to be prepared competitively. For example, by using thiosemicarbazide (TS), pyromellitic dianhydride (PMDA) and toluene-2,4-diisocyanate (TDI), as linkers, the chitosan backbone can be modified to afford preferable structures having diverse and appropriate functional groups than the pristine chitosan.[69–73]

Indeed, PMDA is generally a powerful electrophilic compound due to the presence of anhydride functional groups.[74,75] Consequently, it can react with both $-NH_2$ and –OH functional groups of chitosan to form new amide or ester ones, respectively, as well as free carboxylic acid functional groups. Furthermore, the existence of TS, as a good donor ligand and hydrogen bond-forming moiety, increases the catalytic performance of the as-prepared nanomaterial by strong chelation of Lewis acid catalytic species such as transition metal ions on the surface of modified chitosan.[76,77] On the other hand, TDI can be used as an appropriate linker due to the presence of reactive isocyanate functional groups to combine with both $-NH_2$ and –OH functional groups of chitosan. Therefore, design and facile preparation of new chitosan-based nanomaterials by grafting of PMDA, TS and TDI would be more desirable.[78–82]

"Click Chemistry (CC)", which was firstly introduced in 1999 by K. Barry Sharpless, has emerged in the synthesis of heterocyclic compounds as a fascinating research area. Indeed, this concept resulted in joint awarding the 2022 Nobel Prize in Chemistry to Carolyn R. Bertozzi, Morten Meldal and K. Barry Sharpless for the development of CC and bioorthogonal chemistry. In 2001, Sharpless defined CC reactions as a set of organic transformations with high thermodynamic stimulant energy that pushes them quickly and irreversibly to afford a single reaction product.[83–87] As one of the most well-known CC reactions, 1,3-dipolar azide–alkyne and azide–nitrile cycloaddition reactions are widely used for the synthesis of important heterocyclic compounds, namely triazole and tetrazole derivatives, respectively.[88–92]

Tetrazoles are known as a class of synthetic heterocyclic compounds that comprise a five-membered ring containing four nitrogen and one carbon atoms. Remarkably, since pentazoles are highly explosive even at low temperatures, tetrazoles possess the highest number of nitrogen atoms among the stable heterocycles.[93–95] Furthermore, both donor and acceptor electronic characteristics of tetrazole derivatives arise from their planar ring skeleton as well as the nitrogen-rich multi-electron conjugated system.[96–99] Tetrazoles have a broad range of applications including in medicinal, material and coordination chemistry, organometallic compounds and catalysis technology.[100,101] The tetrazolyl functional group is often considered as a carboxylic acid substitution in drug discovery. Indeed, not only the pK_a of tetrazolyl moiety is close to the –COOH functional group, but also it has nearly the planar delocalized system

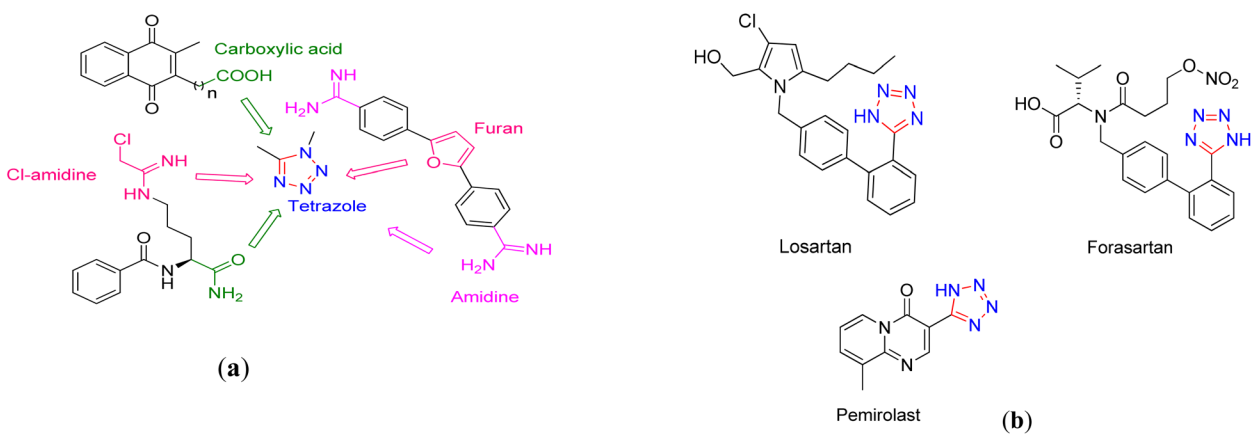

Fig. 1 (a) Tetrazole scaffold as bioisostere of the carboxylic group, Cl-amidine, or heterocyclic furan ring in the medicinal chemistry; (b) active pharmaceutical ingredients having tetrazole moiety: losartan, forasartan, and pemirolast.

space requirements and provides maximum nitrogen content of any heterocyclic compound.[102] Hence, tetrazole moiety can be considered as a bioisosteric alternative analogue for the carboxylic acid, Cl-amidine, or furan ring (Fig. 1a). Consequently, tetrazoles have found applications as antihypertensive,[103] antiviral,[104] antinociceptive,[105] antibacterial,[106] and antiallergic compounds (Fig. 1b) as well as in agriculture and material engineering[107] as herbicides, plant growth regulators, explosives and energy storage devices.[20,23,108–110]

The first tetrazole compound was prepared more than one hundred years ago, and then many scientists have introduced various synthetic strategies for preparation of these compounds. A 1,3-dipolar cycloaddition reaction is the most common method which takes place between azide ion or hydrazoic acid with various simple nitrile derivatives under high pressure.[111] Different catalytic systems have been used in this approach during different decades. Some recent examples consist of the use of zinc(II) salts,[112] copper(I) salt,[113] MCM-41-

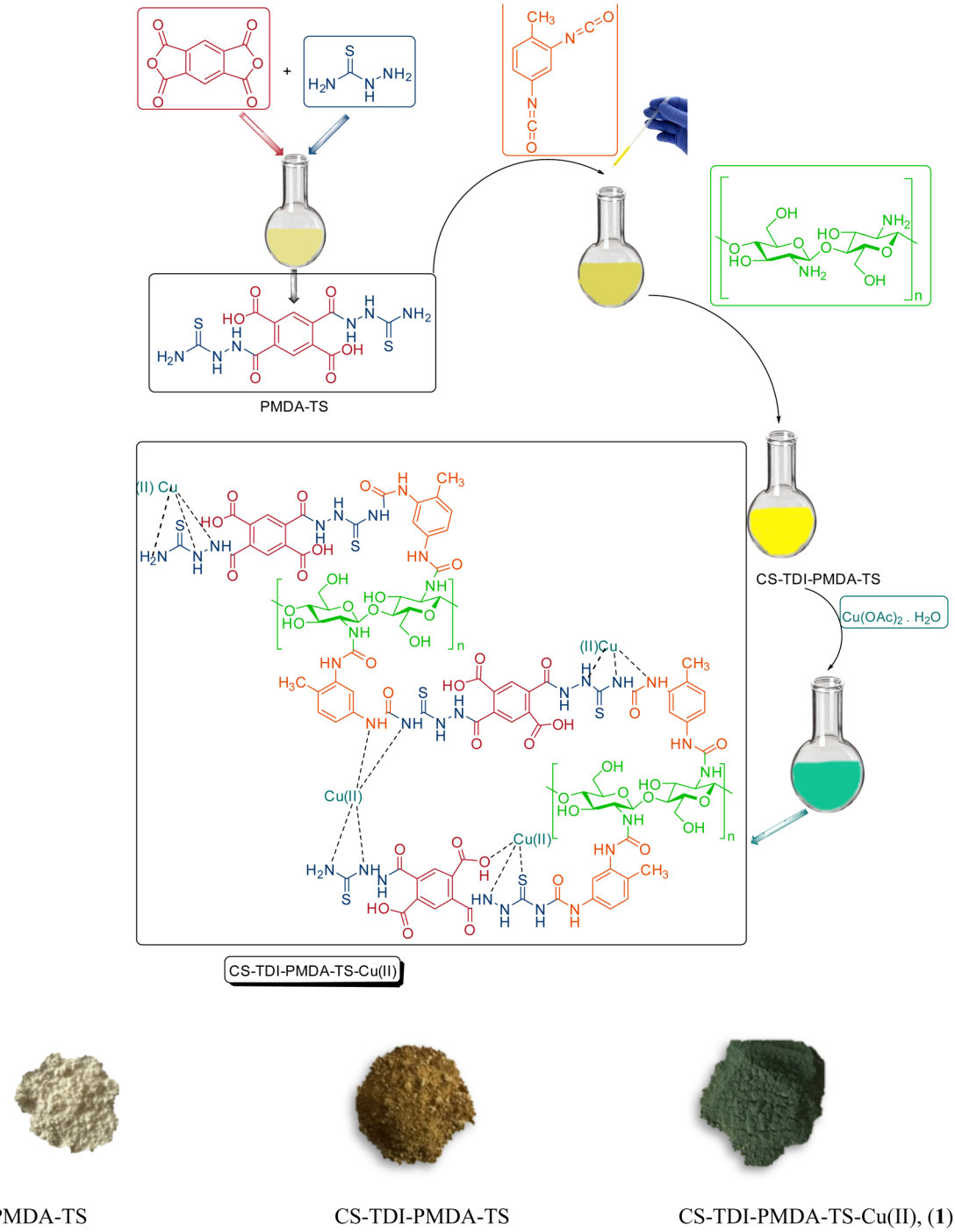

Scheme 1 Schematic preparation of the CS–TDI–PMDA–TS–Cu(II) nanocomposite (**1**).

SO_3H,[114] Fe_3O_4@L-lysine-Pd(0),[115] $FeCl_3$–SiO_2,[116] Zn/Al hydrotalcite,[117] Amberlyst-15 [118,119] and urea-bridged PMO supporting Cu(II) nanoparticles[73] mostly at high temperatures or dialkyl aluminum azides, as the substrate, in the presence of an appropriate catalyst. Indeed, many of these methods suffer from drawbacks for example the use of costly catalytic systems, undesirable yields, the use of toxic and carcinogenic solvents including DMF, long reaction times, and no recycling of the catalyst despite their merits. In continuation of our ongoing studies to explore efficient nanocatalysts for different organic transformations,[9–11,21,22,33,43,66–68,120–123] our attention was deployed to the design and application of supramolecular Cu(II) nanoparticles on a modified chitosan backbone. It contains urea and thiourea bridges using thiosemicarbazide (TS), pyromellitic dianhydride (PMDA) and toluene-2,4-diisocyanate (TDI) linkers (CS–TDI–PMDA–TS–Cu(II), **1**) for the synthesis of tetrazole derivatives through multicomponent cascade Knoevenagel condensation/click 1,3-dipolar azide–nitrile cycloaddition reactions. Various aromatic aldehydes **4a–q** and malononitrile (**2**) were well survived in the presence of nanocomposite **1** to afford corresponding Knoevenagel intermediate and subsequent [3 + 2] cycloaddition desired products **5a–q** by reacting with sodium azide (Scheme 1). Indeed, various tetrazole derivatives **5a–q** were efficiently synthesized using a low loading of CS–TDI–PMDA–TS–Cu(II) nanocatalyst (**1**), as a reusable catalytic system, under solvent-free conditions in short reaction times.

2. Experimental

2.1. Materials and instrumentation

All chemicals and reagents were purchased with high purity from Merck or Aldrich and used as received, except for liquid aldehydes which were distilled before their use. The progress of reactions and the purity of the obtained products were monitored by thin layer chromatography (TLC) using Merck aluminum plates coated with 0.2 mm silica gel F254. Melting points were measured using an electrothermal 9100 device and are uncorrected. Characterization of the CS–TDI–PMDA–TS–Cu(II) nanocatalyst (**1**), as well as identification of products, was performed using KBr discs on a Shimadzu FTIR-8400S spectrometer. A Bruker DRX-500 Avance spectrometer was used for the recording of ^{1}H NMR (500 MHz) spectra of products in DMSO-d_6 at ambient temperature. Thermal gravimetric analysis data were gathered by a Bahr company STA 504 equipment. The X-ray diffraction pattern was carried out using an STOE apparatus with a CuKα radiation source. Field emission scanning electron microscopy images were recorded by a TESCAN-MIRA III device. All the products are known compounds and were identified by comparison of their physical and spectral data with those of authentic samples.

2.2. Preparation of the chitosan modified with urea and thiourea bridges using TS, PMDA and TDI linkers (CS–TDI–PMDA–TS)

In a single-neck round-bottom 20 mL flask equipped with a condenser, a mixture of TS (2.00 mmol) and PMDA (1.00 mmol) in THF (10 mL) was heated under reflux conditions for 24 h. Then, the mixture was cooled to ambient temperature and the obtained white powder was washed with THF and dried at 70 °C for 6 h. The product was dispersed in 20 mL of dry toluene at room temperature. After 30 min of stirring, TDI (1.0 mmol) was added to the prepared mixture dropwise under an argon atmosphere. The mixture was heated in a two-neck round-bottom flask equipped with a condenser under reflux conditions for 12 h. Afterward, CS (0.2 g) was added to the mixture for 36 h under the same conditions. The obtained light-yellow powder was washed with dry toluene and dried at 70 °C for 24 h.

2.3. Preparation of CS–TDI–PMDA–TS–Cu(II) nanocatalyst (1)

At this stage, CS–TDI–PMDA–TS in the presence of copper(II) acetate monohydrate was used to embed copper into the CS–TDI–PMDA–TS backbone. Copper(II) acetate monohydrate (0.2 g) was added to a mixture of the CS–TDI–PMDA–TS (0.4 g) dispersed in EtOH 96% (15 mL) and stirred for 12 h at room temperature. Finally, the light green powder of CS–TDI–PMDA–TS–Cu(II) nanomaterial (**1**) was filtered off and washed with EtOH 96% (3 × 10 mL) and then dried at 70 °C for 24 h.

2.4. General procedure for the synthesis of 5-substituted-1*H*-tetrazoles derivatives 5a–q catalyzed by CS–TDI–PMDA–TS–Cu(II) nanocatalyst (1)

In a screwed test tube, a mixture of aryl aldehyde (**4a–q**, 1.00 mmol), malononitrile (**2**, 1.10 mmol), and sodium azide (**3**, 1.50 mmol) was heated in the presence of CS–TDI–PMDA–TS–Cu(II) nanocatalyst (**1**, 20 mg) under solvent-free conditions at 110 °C in an oil bath and stirred for the time indicated in Table 1. The reaction progress was monitored by TLC (*n*-hexane/EtOAc, 1 : 1). After completion of the reaction, the nanocatalyst **1** was easily separated through filtration of the obtained aqueous mixture by adding of distilled water (2.5 mL). To separate the products, aqueous HCl (2.0 N, 2.5 mL) and EtOAc (3 × 3.0 mL) were added to the filtrate with vigorous stirring. Then, the two-phase mixture was separated using a separatory funnel each time. The desired products **5a–q** were crystallized by adding *n*-hexane and scraping the bottom of the container. After filtering and drying the precipitate at 70 °C, tetrazole compounds **5a–q** were obtained. By employing ^{1}H NMR, and FT-IR spectroscopy and melting point, the as-synthesized compounds **5** were characterized.

2.5. Spectral data of the selected products

2.5.1 (*E*)-3-(2-Chlorophenyl)-2-(1*H*-tetrazole-5-yl) acrylonitrile (5b). Cream solid powder; M_p: 174–176 °C; FT-IR (KBr) ν: 3241, 3025, 2207, 1573, 1475, 973, 824, 672 cm^{-1}; ^{1}H NMR (500 MHz, DMSO-d_6): δ (ppm) 7.55–7.57 (m, 2H), 7.65–7.67 (d, J = 8.4 Hz, 1H), 8.10–8.11 (d, J = 6.3 Hz, 1H), 8.42 (s, 1H, CH), 13.19 (s, 1H, NH).

2.5.2 (*E*)-3-(4-Methoxyphenyl)-2-(1*H*-tetrazole-5-yl) acrylonitrile (5l). Pale yellow powder; M_p: 155–158 °C; FT-IR (KBr) ν: 3148, 2256, 1573, 1416, 1118, 930, 810, 681, 649 cm^{-1}; ^{1}H NMR (500 MHz, DMSO-d_6): δ (ppm) 7.13–7.14 (d, J = 8.3 Hz, 2H), 8.00–8.02 (d, J = 8.3 Hz, 2H), 8.27 (s, 1H, CH), 13.40 (s, 1H, NH).

Table 1 Optimization of the conditions for the synthesis of 1*H*-tetrazoles in the model reaction of malononitrile (**2**), NaN_3 (**3**) and 4-chlorobenzaldehyde (**4a**) under different conditions[a]

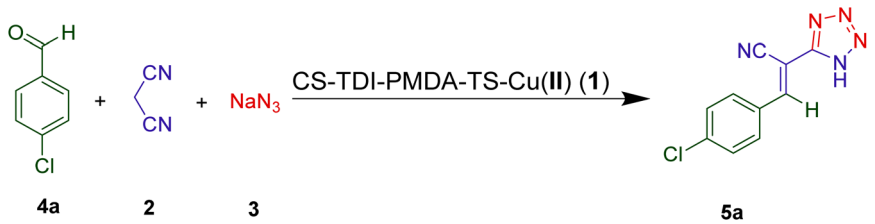

Entry	Catalyst	Catalyst loading (mg)	Solvent	Temperature (°C)	Time (min)	Yield of **5a** (%)[b]
1	—	—	Solvent-free	110	24 h	60
2	—	—	DMF	Reflux	20 h	50
3	CS–TDI–PMDA–TS–Cu(II), (**1**)	10	Solvent-free	110	30	65
4	CS–TDI–PMDA–TS–Cu(II), (**1**)	15	Solvent-free	110	30	80
5	**CS–TDI–PMDA–TS–Cu(II), (1)**	**20**	**Solvent-free**	**110**	**30**	**92**
6	CS–TDI–PMDA–TS–Cu(II), (**1**)	40	Solvent-free	110	45	94
7	CS–TDI–PMDA–TS–Cu(II), (**1**)	20	EtOH	Reflux	60	80
8	CS–TDI–PMDA–TS–Cu(II), (**1**)	20	CH_2Cl_2	Reflux	60	50
9	CS–TDI–PMDA–TS–Cu(II), (**1**)	20	H_2O	Reflux	60	87
10	CS–TDI–PMDA–TS–Cu(II), (**1**)	20	DMF	Reflux	60	90
11	CS–TDI–PMDA–TS–Cu(II), (**1**)	20	EtOAc	Reflux	60	55
12	CS–TDI–PMDA–TS–Cu(II), (**1**)	20	Solvent-free	120	50	93
13	CS–TDI–PMDA–TS–Cu(II), (**1**)	20	Solvent-free	100	70	90
14	CS–TDI–PMDA–TS–Cu(II), (**1**)	20	Solvent-free	80	110	60

[a] Reaction conditions: malononitrile (**2**, 1.10 mmol), sodium azide (**3**, 1.50 mmol), and 4-chlorobenzaldehyde (**4a**, 1.00 mmol) in the presence of CS–TDI–PMDA–TS-Cu(II) nanocatalyst (**1**, 20 mg) and solvent (2.0 mL) unless otherwise noted. [b] Isolated yield.

2.5.3 (*E*)-3-(4-Methylphenyl)-2-(1*H*-tetrazole-5-yl) acrylonitrile (5n). Cream solid powder; M_p: 189–191 °C; FT-IR (KBr) ν: 3029, 2217, 1575, 1556, 1376, 1217, 1174, 813, 609 cm^{-1}; ^1H NMR (500 MHz, DMSO-d_6): δ (ppm) 7.41–7.43 (d, J = 8.0 Hz, 2H), 7.92–7.94 (d, J = 8.0 Hz, 2H), 8.34 (s, 1H, CH), 13.40 (s, 1H, NH).

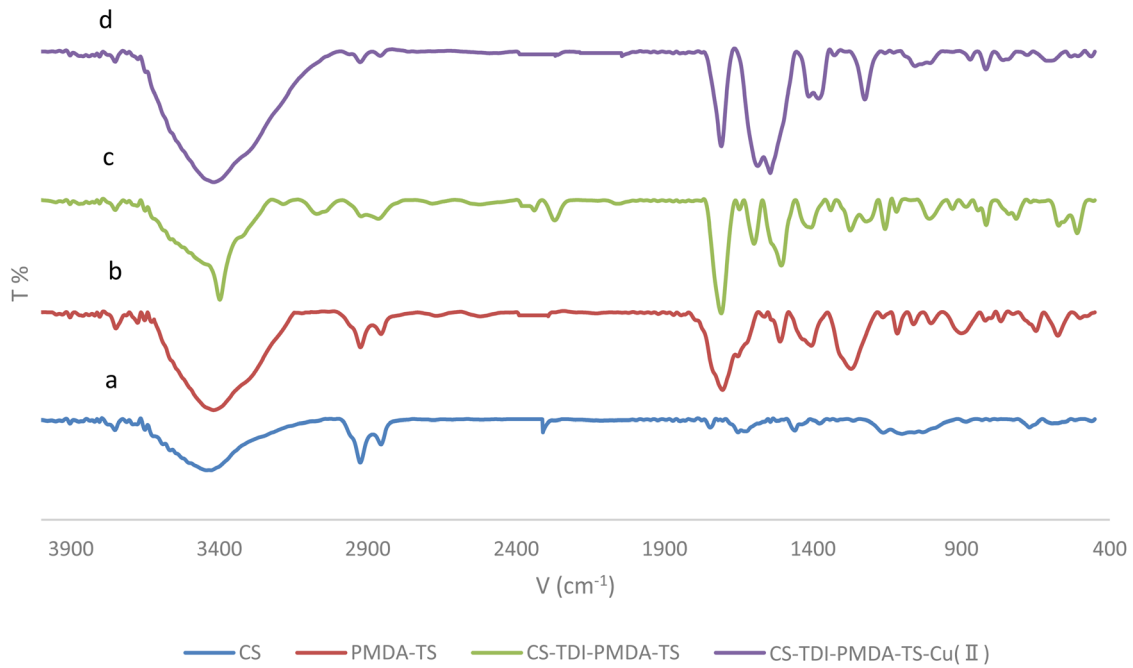

Fig. 2 FT-IR spectra of the commercial CS (a), PMDA–TS (b), CS–TDI–PMDA–TS (c), and the CS–TDI–PMDA–TS–Cu(II) nanocomposite (**1**, d).

3. Results and discussion

3.1. Characterization of the heterogeneous CS–TDI–PMDA–TS–Cu(II) nanocatalyst (1)

After the preparation of the CS–TDI–PMDA–TS–Cu(II) nanomaterial (**1**), its structural, morphological, and textural properties were characterized by using different suitable methods and techniques such as Fourier-transform infrared (FT-IR) spectroscopy, field emission scanning electron microscopy (FESEM), thermogravimetry/differential thermogravimetry analysis (TGA/DTA), energy-dispersive X-ray spectroscopy (EDS), elemental mapping, and X-ray diffraction (XRD).

3.1.1. Fourier transform infrared (FTIR) analysis. In Fig. 2, the FT-IR spectra of commercial chitosan (CS, a), PMDA–TS (b), CS–TDI–PMDA–TS (c), and CS–TDI–PMDA–TS–Cu(II) nanomaterial (**1**, d) have been compared. In Fig. 2a, the stretching vibrations of N–H and O–H bonds of CS appears, as a broad absorption band, at 3100–3426 cm^{-1} in the FT-IR spectra. Also, the C–H stretching vibrations can be seen as the bands at 2926 cm^{-1}. In Fig. 2b the C=S of thiourea group and carbonyl group of carboxylic acid bands are appeared at 1654 cm^{-1} and 1702 cm^{-1}, respectively. In Fig. 2c, the band at 1708 cm^{-1} corresponds to the carbonyl group of carboxylic acid, while the bands at 1622 and 1504 cm^{-1} are assigned to the urea and thiourea groups, respectively. We believe that the small shift in locations of these characteristic bands can be attributed to their interactions with the –OH, $–NH_2$, and N–H groups. The peaks at 1200–1400 cm^{-1} are assigned to the bending of –NH groups. The C–O stretching band is located at about 1100 cm^{-1}. Consequently, the CS containing TS and PMDA by TDI linker were successfully prepared. By interacting the copper(II) species with the surface of catalyst, the vibration signal is observed at 814 cm^{-1}, as shown in Fig. 2d, which confirms the efficient chelation of copper(II) on the modified biopolymeric support's surface.

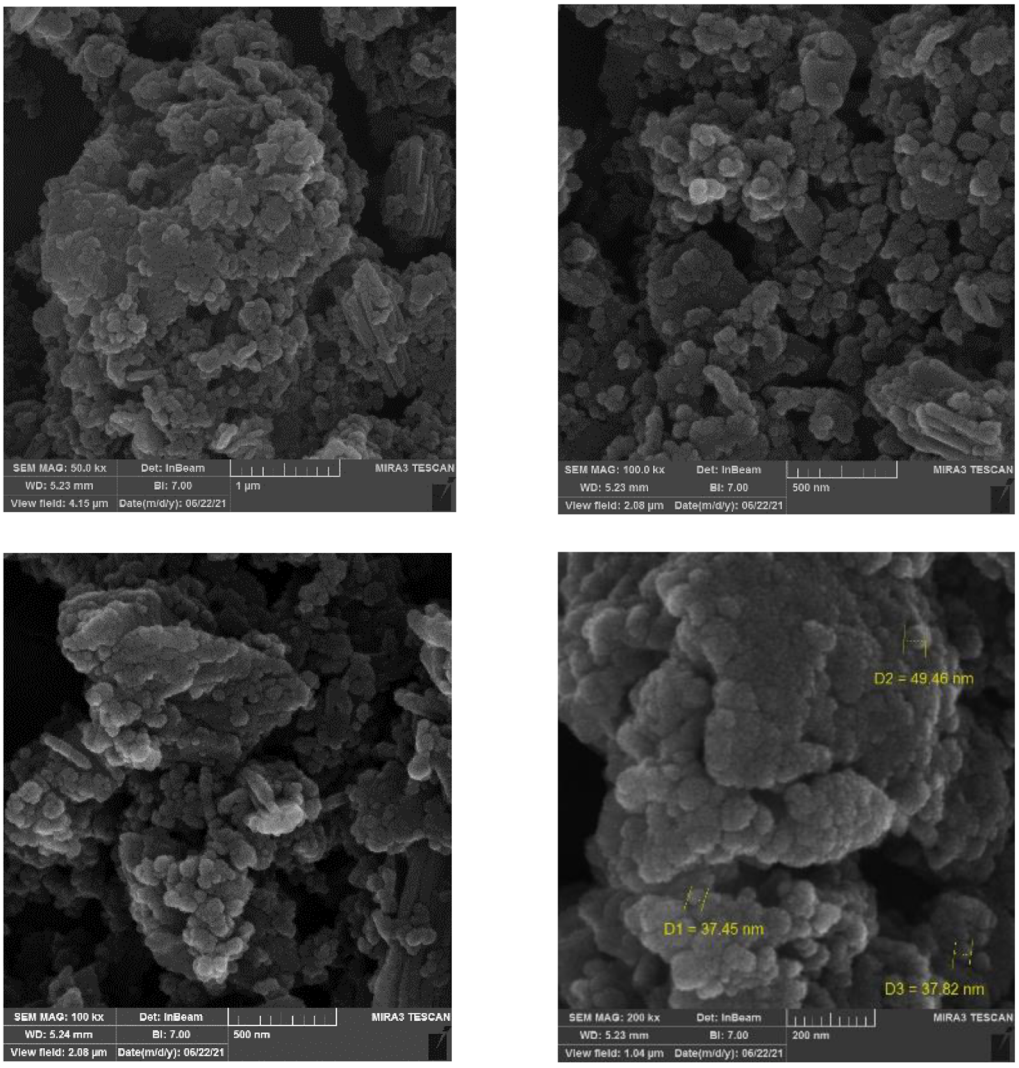

Fig. 3 FESEM images of the CS–TDI–PMDA–TS–Cu(II) nanocomposite (**1**).

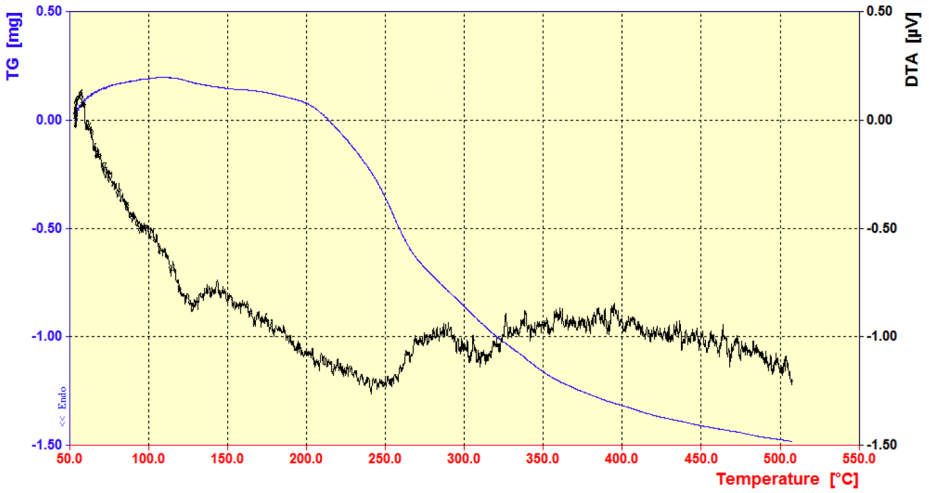

Fig. 4 TGA/DTA analysis of the CS–TDI–PMDA–TS–Cu(II) nanomaterial (**1**).

3.1.2. Scanning electron microscopy (FESEM) analysis. The morphology and particles size distribution of CS–TDI–PMDA–TS–Cu(II) nanomaterial (**1**) were determined by using FESEM technique (Fig. 3). Indeed, the layered modified chitosan backbones are observed obviously while grafted linkers as well as spherical chelated Cu(II) nanoparticles have been distributed on the surface of them. Furthermore, the average particle size is between 37 and 49 nm, denoting uniform distribution of particles and appropriate morphology for the CS–TDI–PMDA–TS–Cu(II) nanocatalyst (**1**).

3.1.3. Thermogravimetric analysis (TGA). The thermogravimetry/differential thermogravimetry analysis (TGA/DTA) were measured for the as-prepared nanocatalyst in the range of 50–500 °C. Fig. 4 demonstrates that the physically adsorbed organic solvents' weight loss of CS–TDI–PMDA–TS–Cu(II) nanocatalyst (**1**) is observed at the range of 50–200 °C. Indeed, physically adsorbed THF, toluene, alcoholic or water molecules which were remained from the preparation steps are removed at first weight loss stage. The next two weight losses of the CS–TDI–PMDA–TS–Cu(II) nanocatalyst (**1**) at 200–500 °C are attributed to the elimination of urea and thiourea bridges grafted onto the surface of chitosan by using TDI and PMDA linkers. These data show the good thermal stability of the CS–TDI–PMDA–TS–Cu(II) nanocomposite (**1**), which is highly significant in the design and application of reusable heterogeneous catalytic systems.

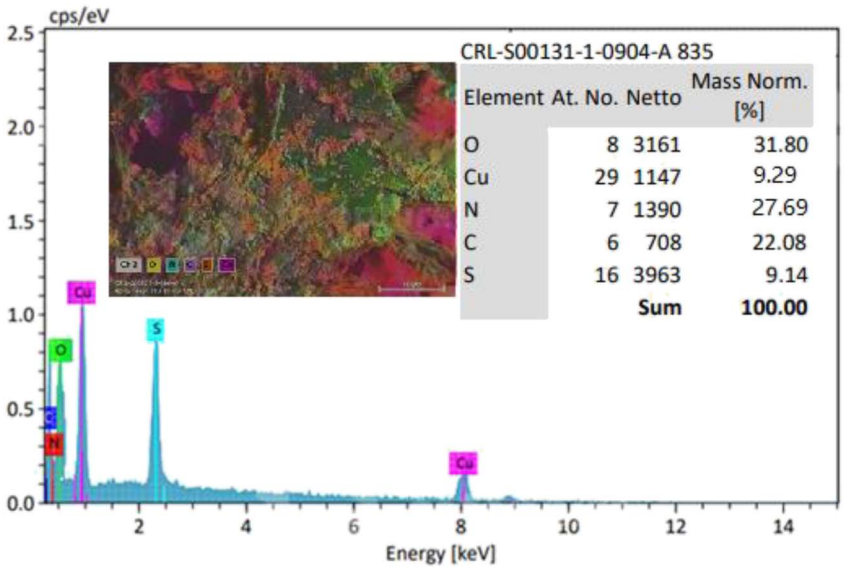

Fig. 5 EDX spectrum of the CS–TDI–PMDA–TS–Cu(II) nanocatalyst (**1**).

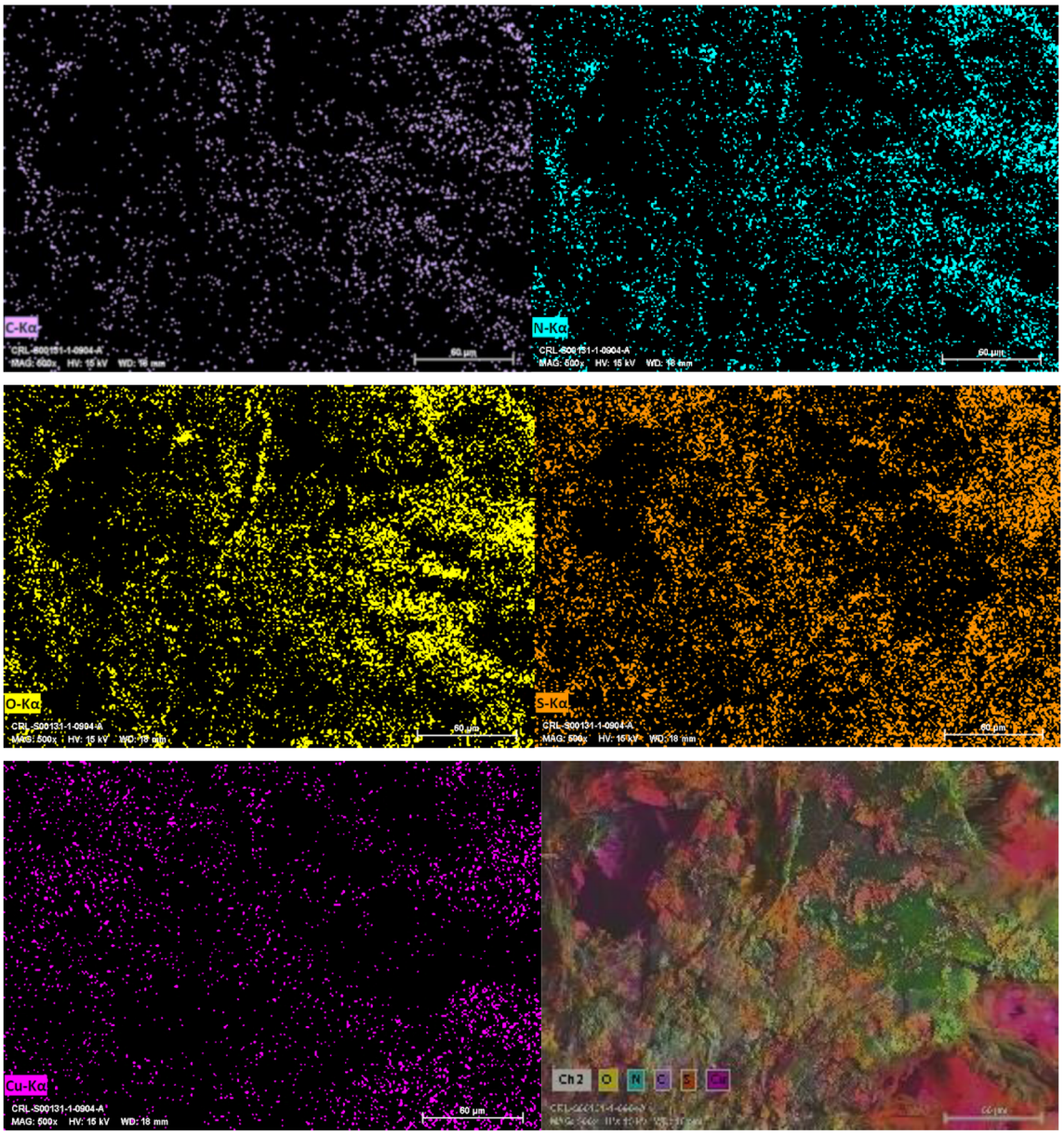

Fig. 6 Elemental mapping of the CS–TDI–PMDA–TS–Cu(II) nanocatalyst (**1**).

3.1.4. Energy dispersive X-ray spectroscopy (EDX) analysis. The composition of nanomaterial **1** was determined by energy dispersive X-ray (EDX) spectroscopy. Fig. 5 shows the EDX spectrum of the nanocomposite **1**. The signals of copper, nitrogen, sulfur, carbon, and oxygen were distinguished in the as-prepared material. In addition, this analysis proves that copper(II) species are well embedded in the structure of nanocatalyst successfully.

3.1.5. Elemental mapping analysis. Another useful technique to demonstrate the distribution of elements in the structure of nanomaterials is elemental mapping. As shown in Fig. 6, the elements of copper, nitrogen, sulfur, carbon, and oxygen are well uniformly distributed throughout the chosen area of the EDX image. This property in the heterogeneous catalytic systems is very important to demonstrate higher catalytic activity at lower concentration of active species such as Cu cations in the structure of CS–TDI–PMDA–TS–Cu(II) nanocatalyst (**1**).

3.1.6. X-Ray diffraction spectroscopy (XRD) analysis. The XRD was also employed to study the crystalline structures of CS–TDI–PMDA–TS–Cu(II) nanocatalyst (**1**). The wide-angle XRD patterns shown in Fig. 7 demonstrate the crystallinity and arrangement of CS–TDI–PMDA–TS–Cu(II) nanocomposite (**1**) and full compliance with the CS (JCPDS card no. 00-039-1894), PMDA (JCPDS card no. 00-024-1864), TS (JCPDS card no. 00-008-0726), copper(II) acetate monohydrate (JCPDS card no. 00-004-0836). Also, chemical modifications led to decrease of peak intensities of the chitosan.

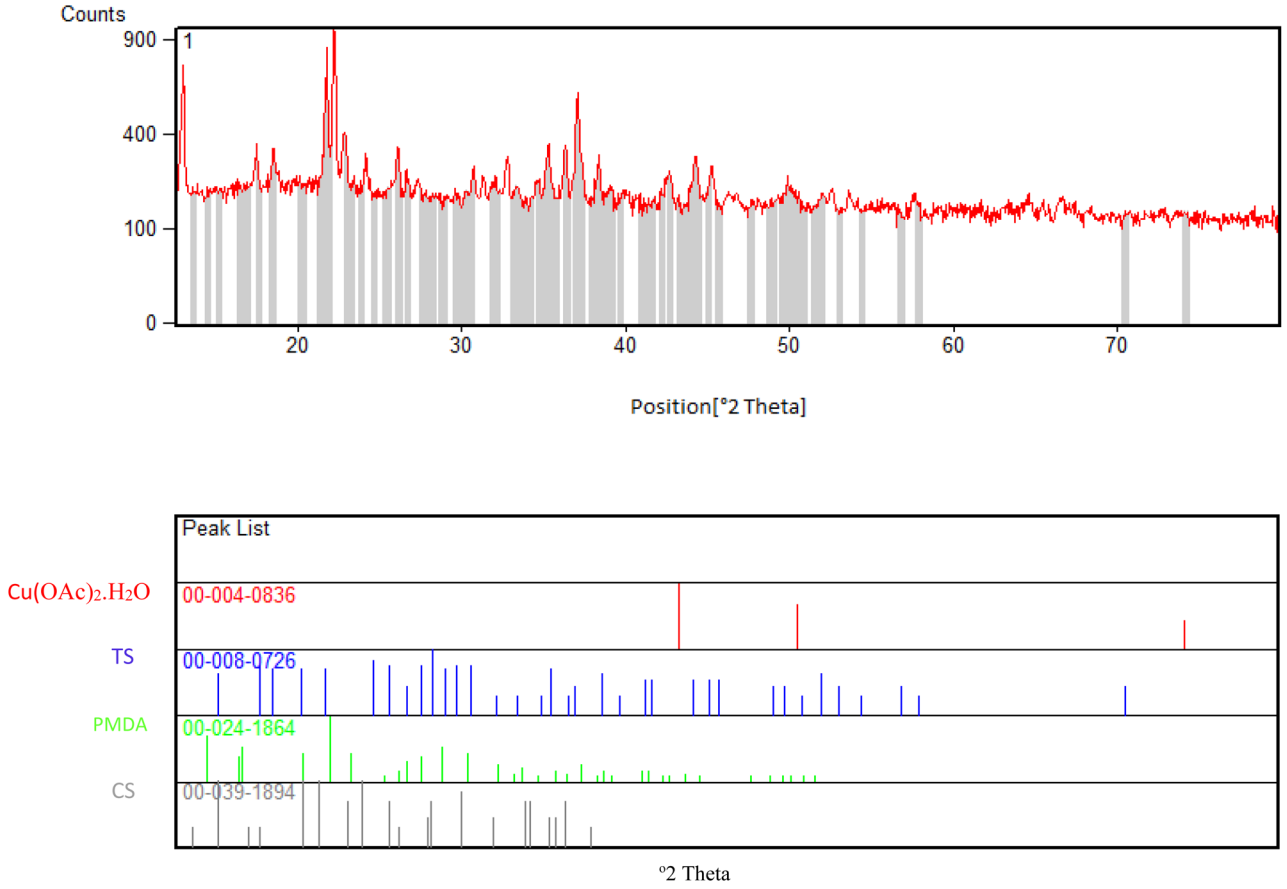

Fig. 7 XRD pattern for the CS–TDI–PMDA–TS–Cu(II) nanocatalyst (**1**).

3.2. Optimization of conditions for the synthesis of tetrazole derivatives in the presence of CS–TDI–PMDA–TS–Cu(II) nanocatalyst (1)

After characterization of the CS–TDI–PMDA–TS–Cu(II) nanocatalyst (**1**), its performance for the preparation of 1*H*-tetrazole derivatives was assessed. Thus, the effect of parameters including various catalyst loadings, temperature, and solvent on the yield and reaction time were studied in this step systematically to recognize optimal conditions for the synthesis of 1*H*-tetrazole derivatives. Therefore, the reaction between 4-chlorobenzaldehyde (**4a**, 1.00 mmol), malononitrile (**2**, 1.10 mmol) and sodium azide (**3**, 1.50 mmol) was chosen as the model reaction in this study. Table 1 summarizes the obtained results. Initially, in the absence of any catalyst, the model reaction was performed in DMF under reflux conditions or solvent-free conditions. The dependency of the obtained yield of the model reaction to the catalyst and temperature was obvious because of moderate yields of the desired product (*E*)-3-(4-chlorophenyl)-2-(1*H*-tetrazole-5-yl) acrylonitrile (**5a**) after prolonged reaction times (entries 1–2, Table 1). Remarkably, the obtained yield of desired product of **5a** was significantly improved in the presence of CS–TDI–PMDA–TS–Cu(II) nanocatalyst (**1**) after very short reaction times (entries 3–6, Table 1). These findings demonstrate appropriate performance of the nanocatalyst **1** in promoting of the model reaction to afford the desired product **5a**, which originates from very good dispersion of active catalytic sites and proper surface area of the CS–TDI–PMDA–TS–Cu(II) nanomaterial (**1**).

In the next step, the effects of different polar and nonpolar solvents as well as solvent-free conditions were examined on the reaction times and yields (Table 1, entries 5 and 7–14). Consequently, when the model reaction was carried out under solvent-free conditions, the best results were achieved (Table 1, entry 5). Furthermore, with decreasing applied temperatures from 120 to 80 °C, the yield of desired product diminishes (Table 1, entries 5 and 12–14). It is noteworthy that when the model reaction was performed at 110 °C, the best results in terms of yield and reaction time were gained. Indeed, higher temperature cannot improve the amount of yield or reaction time (entry 12, Table 1). Furthermore, separation of the nanocatalyst **1** is much easier under solvent-free conditions compared to experiments in different solvents during work-up procedure and remaining the heterogeneous catalyst **1**.

Afterward, the optimized conditions were expanded to other aromatic aldehydes **4b–q** to investigate the scope of reaction for synthesizing of 1*H*-tetrazole derivatives in the presence of CS–TDI–PMDA–TS–Cu(II) nanocatalyst (**1**). A diversity of aromatic carbocyclic or heterocyclic aldehydes **4a–q** well

Table 2 Synthesis of 5-substituted-1*H*-tetrazole derivatives **5a–q** catalyzed by the CS–TDI–PMDA–TS–Cu(II) nanomaterial (**1**)[a]

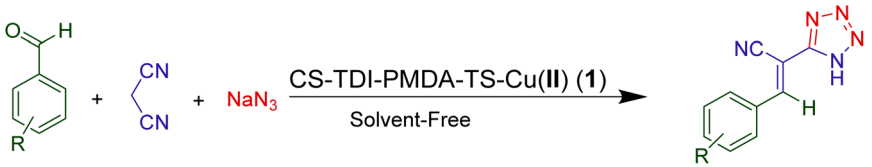

4a-q **2** **3** **5a-q**

Entry	Aldehyde (**4**)	Product (**5**)	Time (min)	Yield[b] (%)	M.p. (°C) [Obs.]	M.p. (°C) [Lit.]
1	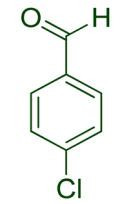 4a	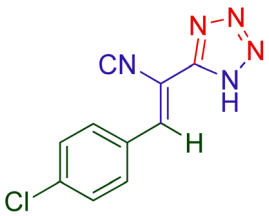 5a	40	92	158–160	156–159 (ref. 20)
2	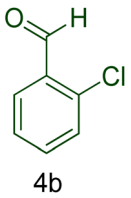 4b	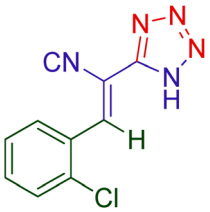 5b	40	90	174–176	175–177 (ref. 124)
3	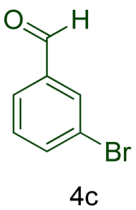 4c	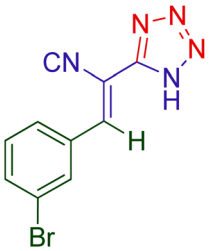 5c	55	90	162–164	161–163 (ref. 125)
4	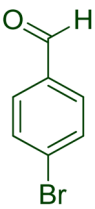 4d	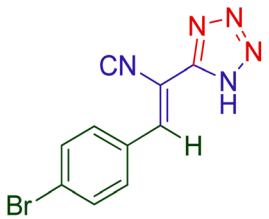 5d	45	92	166–168	166–168 (ref. 126)
5	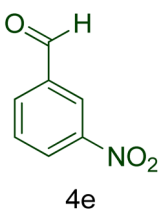 4e	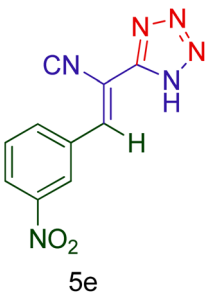 5e	40	85	160–163	161–163 (ref. 127)

Table 2 (*Contd.*)

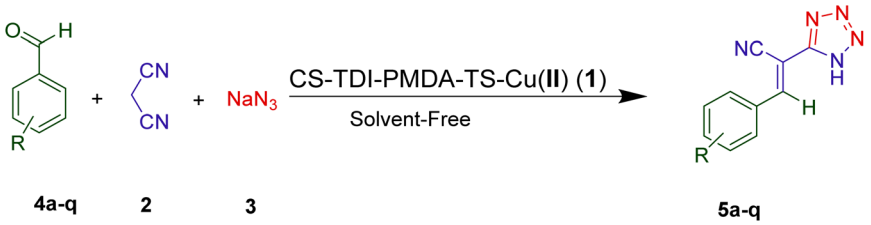

Entry	Aldehyde (4)	Product (5)	Time (min)	Yield[b] (%)	M.p. (°C) [Obs.]	M.p. (°C) [Lit.]
6	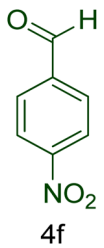 4f	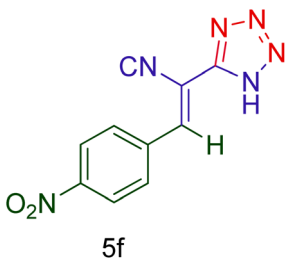 5f	45	88	165–167	166–168 (ref. 128)
7	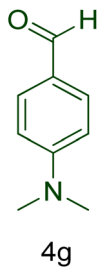 4g	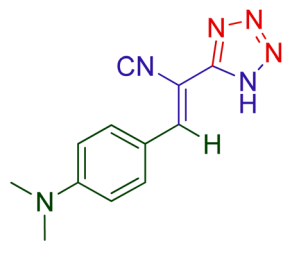 5g	50	92	169–172	169–171 (ref. 20)
8	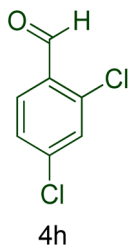 4h	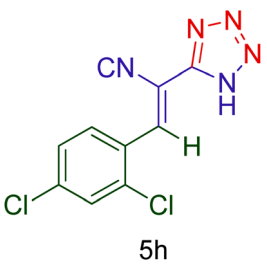 5h	40	90	142–145	142–144 (ref. 20)
9	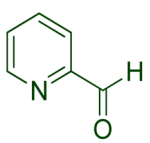 4i	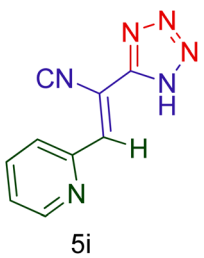 5i	60	86	185–187	185–186 (ref. 20)
10	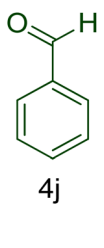 4j	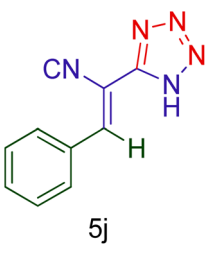 5j	30	90	164–166	164–166 (ref. 127)

Table 2 (*Contd.*)

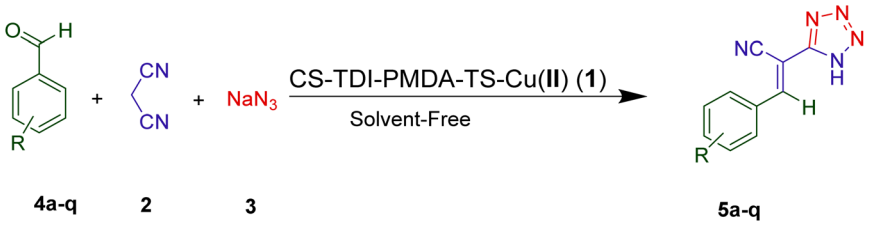

Entry	Aldehyde (4)	Product (5)	Time (min)	Yield[b] (%)	M.p. (°C) [Obs.]	M.p. (°C) [Lit.]
11	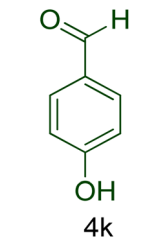 4k	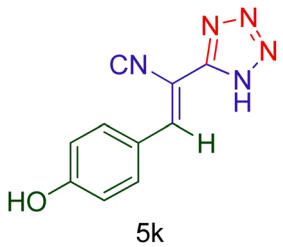 5k	55	82	162–165	161–164 (ref. 20)
12	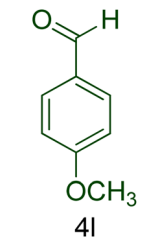 4l	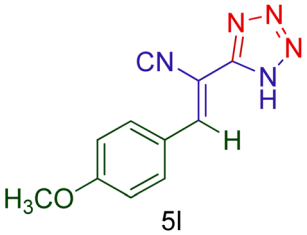 5l	55	90	155–158	156–160 (ref. 20)
13	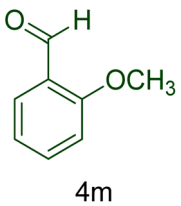 4m	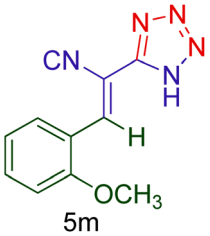 5m	50	86	157–159	157–159 (ref. 20)
14	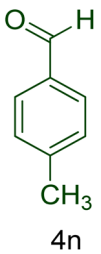 4n	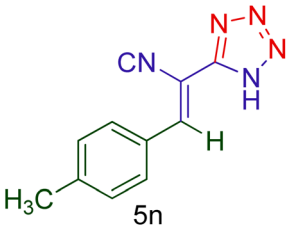 5n	50	88	189–191	190–192 (ref. 110)
15	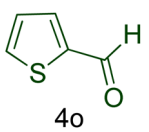 4o	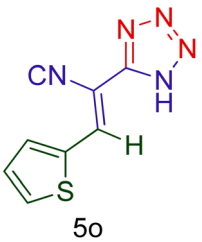 5o	55	82	132–137	132–137 (ref. 110)

Table 2 (*Contd.*)

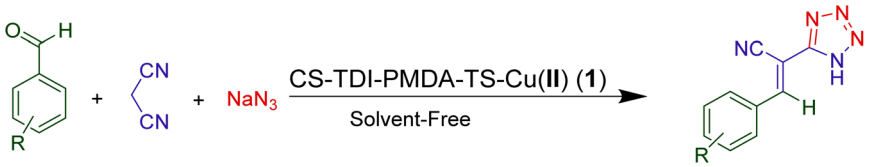

4a-q 2 3 5a-q

Entry	Aldehyde (4)	Product (5)	Time (min)	Yield[b] (%)	M.p. (°C) [Obs.]	M.p. (°C) [Lit.]
16	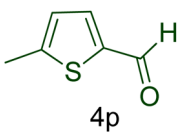 4p	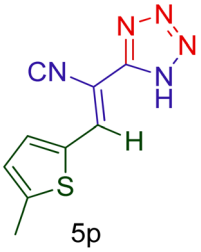 5p	60	88	136–139	135–140 (ref. 110)
17	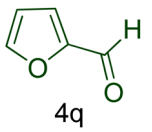 4q	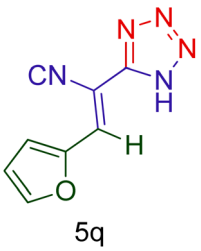 5q	70	88	253–256	253–254 (ref. 20)

[a] Reaction conditions: malononitrile (**2**, 1.10 mmol), sodium azide (**3**, 1.50 mmol), aryl aldehyde (**4a–q**, 1.00 mmol) in the presence of CS–TDI–PMDA–TS–Cu(II) nanocatalyst (**1**, 20 mg), 110 °C under solvent-free conditions. [b] Isolated yields.

survived to involve smoothly in the optimized conditions. As can be observed in Table 2, high to excellent yields were obtained for the desired products **5a–q** within very short reaction times. Accordingly, aromatic aldehydes with a carbocyclic ring bearing electron withdrawing groups **4a–h** or electron-deficient heterocycle **4i** were examined (entries 1–9, Table 2). On the other hand, aromatic aldehydes with a carbocyclic ring bearing electron donating groups **4j–q** as well as electron-rich heterocycle **4o** were studied to involve in the optimized conditions to afford corresponding 1*H*-tetrazole derivatives **5j–q** (entries 10–17, Table 2). Indeed, the required reaction time for completion is usually lower for the aldehydes containing an electron-withdrawing group compared to those ones having a donor group. This implies that formation of the Knoevenagel intermediate is the rate-determining step for all studied aldehydes.

3.3. Proposed mechanism for the preparation of 5-substituted-1*H*-tetrazole derivatives catalyzed by CS–TDI–PMDA–TS–Cu(II) nanocatalyst (1)

A plausible mechanism for the one-pot synthesis of (*E*)-2-(1*H*-tetrazole-5-yl)-3-aryl/heteroarylacrylenenitrile derivatives **5a–q** using CS–TDI–PMDA–TS–Cu(II) nanocatalyst (**1**) is shown in Scheme 2. Initially, the aromatic aldehydes **4** are activated by CS–TDI–PMDA–TS–Cu(II) nanocatalyst (**1**) step by step to condensate with the nucleophilic tautomer of malononitrile (**2′**) having C–H acids and affording Knoevenagel intermediate (**II**).[129] In order to form the 5-membered tetrazole ring, the activated aryl/heteroarylidine malononitrile Knoevenagel intermediate (**II**) by the nanocatalyst **1** is subsequently involved in a cascade reaction with sodium azide (**3**) through the concerted [3 + 2] cycloaddition to afford corresponding tetrazole sodium salt (**III**). Finally, the desired tetrazole derivatives are formed by the addition of HCl (aq). Furthermore, the CS–TDI–PMDA–TS–Cu(II) nanocatalyst (**1**) is liberated and can start next catalytic cycle.

3.4. Comparison of the catalytic activity of CS–TDI–PMDA–TS–Cu(II) nanocatalyst (1) in the synthesis of tetrazole derivatives with other catalytic systems

A comparison of the previously reported methods for the synthesis of tetrazole **5a** with the present protocol is shown in Table 3. It is apparent that high to excellent yields, short reaction time, and avoiding the use of toxic or carcinogenic solvents

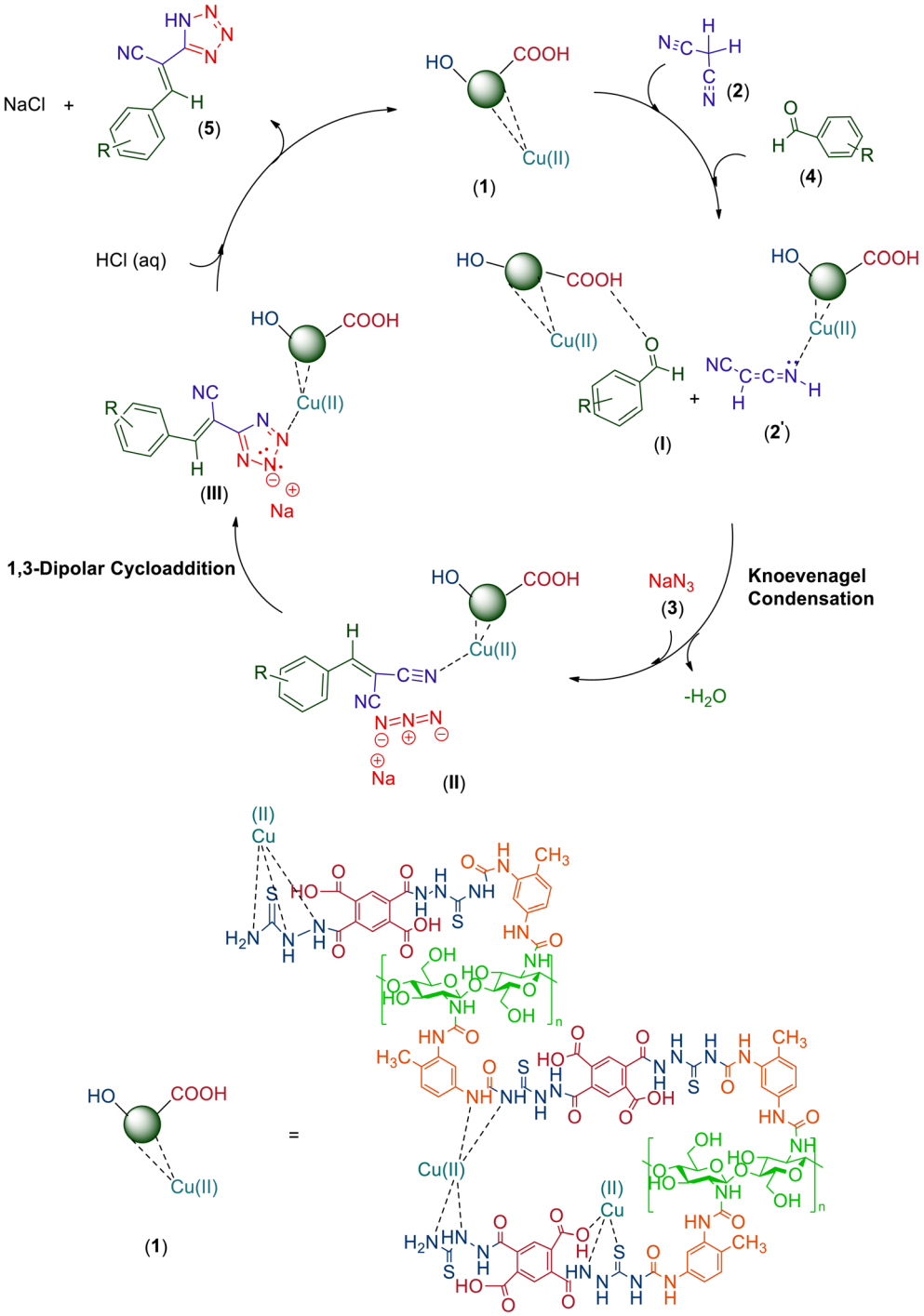

Scheme 2 The proposed mechanism for the synthesis of tetrazole derivatives **5** catalyzed by the heterogeneous supramolecular CS–TDI–PMDA–TS–Cu(II)nanocatalyst (**1**).

such as DMF is the advantages of the present protocol compared to the most of previously reported methods.

3.5. Examining the recyclability of CS–TDI–PMDA–TS–Cu(II) nanocatalyst (1) for the synthesis of 5-substituted-1*H*-tetrazole derivatives 5

Currently, reusability is a significant parameter in the field of nano-ordered heterogeneous catalytic systems to address green and sustainable chemistry principles and reducing the impact of chemical processes on the environment. In this context, the recyclability of as-prepared CS–TDI–PMDA–TS–Cu(II) nanocatalyst **1** was assessed under optimal conditions for the model reaction. Hence, after the completion of the model reaction, the nanocatalyst **1** was easily separated by filtration after addition of aqueous HCl. Then, the recycled CS–TDI–PMDA–TS–Cu(II) nanocatalyst (**1**) was dispersed in EtOH and H_2O for 15 min, respectively. The recycled catalyst was kept in an oven at 70 °C

Table 3 Comparison of the catalytic efficiency of the CS–TDI–PMDA–TS–Cu(II) nanocatalyst (**1**) with other catalytic systems

Entry	Catalyst	Catalyst loading	Reaction conditions	Time (h)	Yield (%)	Reference
1	**CS–TDI–PMDA–TS–Cu(II), (1)**	**20.0 mg**	**Solvent-free/110 °C**	**30 min**	**92**	**Present work**
2	Nano-Fe_3O_4	20 mol%	Solvent-free/80 °C	4.5	90	124
3	Fe_3O_4@fibroin–SO_3H	10 mol%	Solvent-free/100 °C	2.0	86	130
4	Fe_3O_4–CNT–SO_3H nanocomposite	20.0 mg	Solvent-free/80 °C	2.5	90	131
5	NiO nanoparticles	4.5 mg	DMF/70 °C	6.0	90	132
6	NH–Cu(II)@MNP	20.0 mg	EtOH/80 °C	5.0	92	133
7	Zn (mettalic)	130.7 mg	H_2O/50 °C	3.0	68	134
8	$(CuOTf)_2 \cdot C_6H_6$	36.2 mg	Toluene/r.t.	7.0	81	135
9	$Fe(OAc)_2$	17.4 mg	DMF/H_2O (9 : 1) 80 °C	24.0	89	136
10	OPNSA	45.4 mg	Solvent-free/100 °C	10.0	80	137

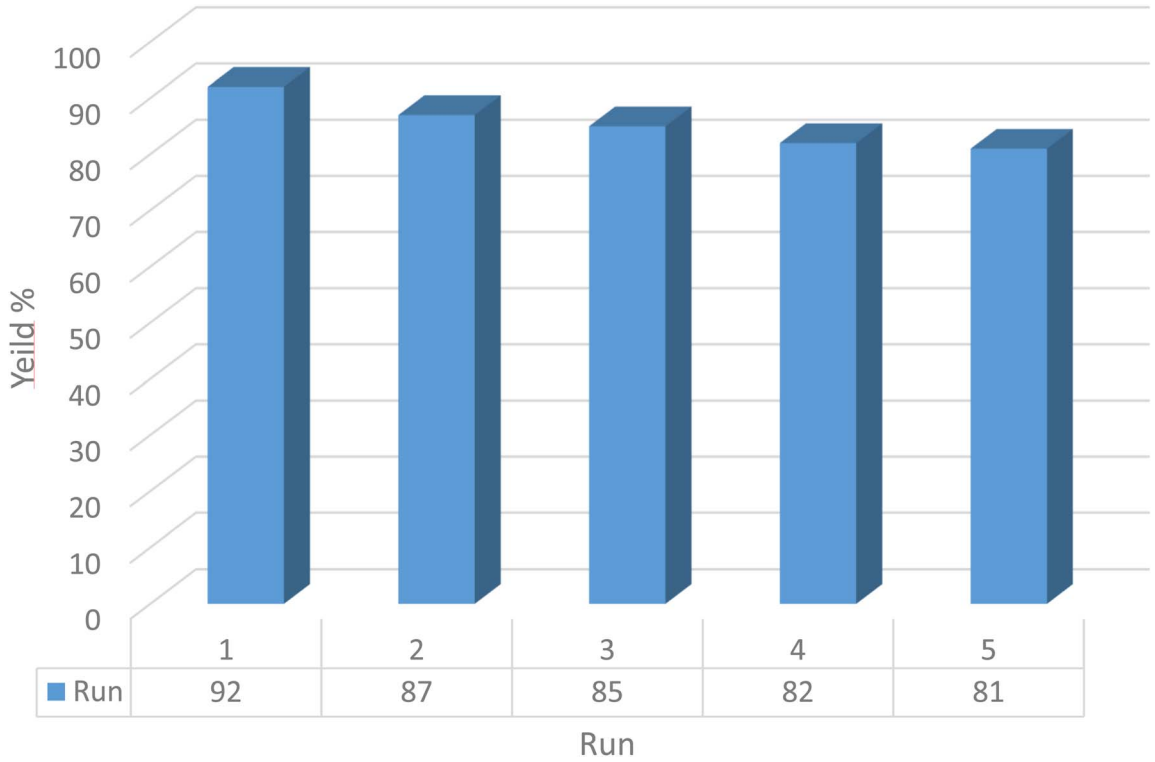

Fig. 8 Reusability data for the CS–TDI–PMDA–TS–Cu(II) nanocatalyst (**1**) in the synthesis of **5a**.

for one hour and reused for the next run under optimized conditions. Fig. 8 provides the results of the catalyst recycling for five consecutive runs. As data in Fig. 8 demonstrate, a little decrease in the reaction yield was observed in each run under optimized conditions. These data indicate the capability of the catalyst to be reused with structural stability and high efficiency.

4. Conclusions

In conclusion, a new supramolecular CS–TDI–PMDA–TS–Cu(II) nanocomposite based on the naturally occurring chitosan biopolymer with urea and thiourea bridges was designed, easily prepared, and fully characterized by appropriate spectroscopic and analytical methods or techniques used for nanomaterials. The catalytic activity of CS–TDI–PMDA–TS–Cu(II) nanomaterial was demonstrated in the one-pot synthesis of tetrazole derivatives through cascade Knoevenagel condensation and concerted 1,3-cycloaddition reactions as a representative of the Click Chemistry concept. The desired 5-substituted-1*H*-tetrazole derivatives were prepared under solvent-free conditions in good purity and high to excellent yields under mild conditions. Low catalyst loading, solvent-free conditions, very short reaction times, and reusability of the catalyst for at least five consecutive runs without significant loss of its activity can be considered as desirable features of this new protocol.

Conflicts of interest

There are no conflicts to declare.

Acknowledgements

We are grateful for the financial support from The Research Council of Iran University of Science and Technology (IUST), Tehran, Iran (Grant No. 160/22061) for their support. We would also like to acknowledge the support of The Iran Nanotechnology Initiative Council (INIC), Iran.

References

1 T. Chen, Y. Peng, M. Qiu, C. Yi and Z. Xu, *Nanoscale*, 2023, **15**, 3594–3609.
2 Y. Pei, L. Wang, K. Tang and D. L. Kaplan, *Adv. Funct. Mater.*, 2021, **31**, 2008552.
3 H. Mittal, S. S. Ray, B. S. Kaith, J. K. Bhatia, J. Sharma and S. M. Alhassan, *Eur. Polym. J.*, 2018, **109**, 402–434.
4 G. Crini, *Environ. Chem. Lett.*, 2019, **17**, 1623–1643.
5 J. Wróblewska-Krepsztul, T. Rydzkowski, I. Michalska-Pożoga and V. K. Thakur, *Nanomaterials*, 2019, **9**, 404.
6 L. Zhang, Y. Yang, J. Tan and Q. Yuan, *Mater. Chem. Front.*, 2020, **4**, 1315–1327.
7 D. Das and S. Pal, *RSC Adv.*, 2015, **5**, 25014–25050.
8 M. Dohendou, K. Pakzad, Z. Nezafat, M. Nasrollahzadeh and M. G. Dekamin, *Int. J. Biol. Macromol.*, 2021, **192**, 771–819.
9 E. Valiey, M. G. Dekamin and S. Bondarian, *RSC Adv.*, 2023, **13**, 320–334.
10 M. G. Dekamin, M. Azimoshan and L. Ramezani, *Green Chem.*, 2013, **15**, 811–820.
11 M. Dohendou, M. G. Dekamin and D. Namaki, *Nanoscale Adv.*, 2023, **5**, 3463–3484.
12 V. S. Shende, V. B. Saptal and B. M. Bhanage, *Chem. Rec.*, 2019, **19**, 2022–2043.
13 D. Cole-Hamilton and R. Tooze, in *Catalyst Separation, Recovery and Recycling*, Springer, 2006, pp. 1–8.
14 C. J. Brown, F. D. Toste, R. G. Bergman and K. N. Raymond, *Chem. Rev.*, 2015, **115**, 3012–3035.
15 S. Reimann, J. Stötzel, R. Frahm, W. Kleist, J.-D. Grunwaldt and A. Baiker, *J. Am. Chem. Soc.*, 2011, **133**, 3921–3930.
16 J. H. Clark, in *Handbook of Green Chemistry and Technology*, 2002, pp. 1–9, DOI: 10.1002/9780470988305.ch1.
17 K. Bourikas, H. K. Matralis, C. Kordulis and A. Lycourghiotis, *J. Phys. Chem.*, 1996, **100**, 11711–11719.
18 A. Alinasab Amiri, S. Javanshir, Z. Dolatkhah and M. G. Dekamin, *New J. Chem.*, 2015, **39**, 9665–9671.
19 M. G. Dekamin and Z. Mokhtari, *Tetrahedron*, 2012, **68**, 922–930.
20 S. Safapoor, M. G. Dekamin, A. Akbari and M. R. Naimi-Jamal, *Sci. Rep.*, 2022, **12**, 10723.
21 S. Karami, M. G. Dekamin, E. Valiey and P. Shakib, *New J. Chem.*, 2020, **44**, 13952–13961.
22 M. G. Dekamin, E. Kazemi, Z. Karimi, M. Mohammadalipoor and M. R. Naimi-Jamal, *Int. J. Biol. Macromol.*, 2016, **93**, 767–774.
23 E. Valiey and M. G. Dekamin, *Sci. Rep.*, 2022, **12**, 18139.
24 M. Dohendou, M. G. Dekamin and D. Namaki, *Nanoscale Adv.*, 2023, **5**, 2621–2638.
25 B. Fattahi and M. G. Dekamin, *Colloid Interface Sci. Commun.*, 2023, **54**, 100711.
26 T. Fazal, B. N. Murtaza, M. Shah, S. Iqbal, M. Rehman, F. Jaber, A. A. Dera, N. S. Awwad and H. A. Ibrahium, *RSC Adv.*, 2023, **13**, 23087–23121.
27 Y. Wang, Y. Xiong, J. Wang and X. Zhang, *Catal. Commun.*, 2017, **90**, 14–18.
28 K. Parvanak Boroujeni and P. Tahani, *Inorg. Nano-Met. Chem.*, 2017, **47**, 1150–1156.
29 K. Bahrami and M. Khodamorady, *Catal. Lett.*, 2019, **149**, 688–698.
30 M. Khodamorady and K. Bahrami, *Catal. Lett.*, 2020, **150**, 1571–1590.
31 Z. Alirezvani, M. G. Dekamin and E. Valiey, *ACS Omega*, 2019, **4**, 20618–20633.
32 A. Yaghoubi and M. G. Dekamin, *ChemistrySelect*, 2017, **2**, 9236–9243.
33 M. G. Dekamin, F. Mehdipoor and A. Yaghoubi, *New J. Chem.*, 2017, **41**, 6893–6901.
34 S. Hasanzadeh Banakar, M. G. Dekamin and A. Yaghoubi, *New J. Chem.*, 2018, **42**, 14246–14262.
35 N. Norouzi, M. K. Das, A. J. Richard, A. A. Ibrahim, H. M. El-Kaderi and M. S. El-Shall, *Nanoscale*, 2020, **12**, 19191–19202.
36 J. Liang, Z. Liang, R. Zou and Y. Zhao, *Adv. Mater.*, 2017, **29**, 1701139.
37 R. Schlögl, *Angew. Chem., Int. Ed.*, 2015, **54**, 3465–3520.
38 C. M. Friend and B. Xu, *Acc. Chem. Res.*, 2017, **50**, 517–521.
39 T. Jin, T. Liu, E. Lam and A. Moores, *Nanoscale Horiz.*, 2021, **6**, 505–542.
40 S. S. Khutsishvili, T. y. V. Ganenko and B. G. Sukhov, *J. Carbohydr. Chem.*, 2021, 1–15.
41 C. P. Jiménez-Gómez and J. A. Cecilia, *Molecules*, 2020, **25**, 3981.
42 P. S. Bakshi, D. Selvakumar, K. Kadirvelu and N. Kumar, *Int. J. Biol. Macromol.*, 2020, **150**, 1072–1083.
43 Z. Alirezvani, M. G. Dekamin, F. Davoodi and E. Valiey, *ChemistrySelect*, 2018, **3**, 10450–10463.
44 M. Miceli, P. Frontera, A. Macario and A. Malara, *Catalysts*, 2021, **11**, 591.
45 H.-J. Qiu, H.-T. Xu, L. Liu and Y. Wang, *Nanoscale*, 2015, **7**, 386–400.
46 J. Govan and Y. K. Gun'ko, *Nanomaterials*, 2014, **4**, 222–241.
47 L. A. Kolahalam, I. K. Viswanath, B. S. Diwakar, B. Govindh, V. Reddy and Y. Murthy, *Mater. Today: Proc.*, 2019, **18**, 2182–2190.
48 T. A. Saleh, *Environ. Technol. Innovation*, 2020, **20**, 101067.
49 N. Narayan, A. Meiyazhagan and R. Vajtai, *Materials*, 2019, **12**, 3602.
50 J. R. Peralta-Videa, L. Zhao, M. L. Lopez-Moreno, G. de la Rosa, J. Hong and J. L. Gardea-Torresdey, *J. Hazard. Mater.*, 2011, **186**, 1–15.
51 D. Astruc, *Chem. Rev.*, 2020, **120**, 461–463.
52 N. Baig, I. Kammakakam and W. Falath, *Mater. Adv.*, 2021, **2**, 1821–1871.
53 B. Goswami, *Int. J. Nanomater. and Nanostruct.*, 2021, **7**, 13–18.

54 K. Hemalatha, G. Madhumitha, A. Kajbafvala, N. Anupama, R. Sompalle and S. Mohana Roopan, *J. Nanomater.*, 2013, **2013**, 341015.
55 S. R. Attar and S. B. Kamble, *Nanoscale*, 2022, **14**, 16761–16786.
56 F. Ganjali, A. Kashtiaray, S. Zarei-Shokat, R. Taheri-Ledari and A. Maleki, *Nanoscale Adv.*, 2022, **4**, 1263–1307.
57 M. B. Gawande, A. K. Rathi, J. Tucek, K. Safarova, N. Bundaleski, O. M. Teodoro, L. Kvitek, R. S. Varma and R. Zboril, *Green Chem.*, 2014, **16**, 4137–4143.
58 E. Colusso and A. Martucci, *J. Mater. Chem. C*, 2021, **9**, 5578–5593.
59 S. B. Singh and P. K. Tandon, *J. Energy Chem. Eng.*, 2014, **2**, 106–115.
60 V. Polshettiwar and R. S. Varma, *Green Chem.*, 2010, **12**, 743–754.
61 M. Zvaigzne, P. Samokhvalov, Y. K. Gun'ko and I. Nabiev, *Nanoscale*, 2021, **13**, 20354–20373.
62 T. Freire, L. M. Dutra, D. Queiroz, N. Ricardo, K. Barreto, J. Denardin, F. R. Wurm, C. Sousa, A. Correia and P. de Lima-Neto, *Carbohydr. Polym.*, 2016, **151**, 760–769.
63 S. G. Kou, L. M. Peters and M. R. Mucalo, *Int. J. Biol. Macromol.*, 2021, **169**, 85–94.
64 W. Wang, C. Xue and X. Mao, *Int. J. Biol. Macromol.*, 2020, **164**, 4532–4546.
65 H. El Knidri, R. Belaabed, A. Addaou, A. Laajeb and A. Lahsini, *Int. J. Biol. Macromol.*, 2018, **120**, 1181–1189.
66 N. Rostami, M. G. Dekamin, E. Valiey and H. Fanimoghadam, *Sci. Rep.*, 2022, **12**, 8642.
67 N. Rostami, M. G. Dekamin and E. Valiey, *Carbohydr. Polym. Technol. Appl.*, 2023, **5**, 100279.
68 Z. Alirezvani, M. G. Dekamin and E. Valiey, *Sci. Rep.*, 2019, **9**, 17758.
69 M. Ahmad, S. Ahmed, B. L. Swami and S. Ikram, *Carbohydr. Polym.*, 2015, **132**, 164–172.
70 M. Li, Z. Zhang, R. Li, J. J. Wang and A. Ali, *Int. J. Biol. Macromol.*, 2016, **86**, 876–884.
71 Y.-c. Lin, H.-p. Wang, F. Gohar, M. H. Ullah, X. Zhang, D.-f. Xie, H. Fang, J. Huang and J.-x. Yang, *Int. J. Biol. Macromol.*, 2017, **95**, 476–483.
72 S. P. G. Zaferani, M. R. S. Emami, M. K. Amiri and E. Binaeian, *Int. J. Biol. Macromol.*, 2019, **139**, 307–319.
73 E. Valiey and M. G. Dekamin, *Nanoscale Adv.*, 2022, **4**, 294–308.
74 J. Deng, Y. Liu, S. Liu, G. Zeng, X. Tan, B. Huang, X. Tang, S. Wang, Q. Hua and Z. Yan, *J. Colloid Interface Sci.*, 2017, **506**, 355–364.
75 M. Mohammadikish, M. Masteri-Farahani and S. Mahdavi, *J. Magn. Magn. Mater.*, 2014, **354**, 317–323.
76 G. Zhang, Y. Zhou, Z. Ding, L. Fu and S. Wang, *RSC Adv.*, 2017, **7**, 55215–55223.
77 M. Mozaffari, M. R. S. Emami and E. Binaeian, *Int. J. Biol. Macromol.*, 2019, **123**, 457–467.
78 Y. Xing, X.-M. Sun and B.-H. Li, *Environ. Eng. Sci.*, 2009, **26**, 551–558.
79 R. Huang, G. Chen, M. Sun, Y. Hu and C. Gao, *J. Membr. Sci.*, 2006, **286**, 237–244.
80 K. M. Zia, S. Anjum, M. Zuber, M. Mujahid and T. Jamil, *Int. J. Biol. Macromol.*, 2014, **66**, 26–32.
81 F. Kara, E. A. Aksoy, Z. Yuksekdag, N. Hasirci and S. Aksoy, *Carbohydr. Polym.*, 2014, **112**, 39–47.
82 M. A. Javaid, R. A. Khera, K. M. Zia, K. Saito, I. A. Bhatti and M. Asghar, *Int. J. Biol. Macromol.*, 2018, **115**, 375–384.
83 Z. P. Demko and K. B. Sharpless, *Angew. Chem.*, 2002, **114**, 2217–2220.
84 J. Kaur, M. Saxena and N. Rishi, *Bioconjugate Chem.*, 2021, **32**, 1455–1471.
85 C. D. Hein, X.-M. Liu and D. Wang, *Pharm. Res.*, 2008, **25**, 2216–2230.
86 I. Tijunelyte, E. Guenin, N. Lidgi-Guigui, F. Colas, J. Ibrahim, T. Toury and M. Lamy de la Chapelle, *Nanoscale*, 2016, **8**, 7105–7112.
87 J. Nicks and J. A. Foster, *Nanoscale*, 2022, **14**, 6220–6227.
88 Y. Shi, X. Cao and H. Gao, *Nanoscale*, 2016, **8**, 4864–4881.
89 H. A. Younus, M. Al-Rashida, A. Hameed, M. Uroos, U. Salar, S. Rana and K. M. Khan, *Expert Opin. Ther. Pat.*, 2021, **31**, 267–289.
90 S. E. John, S. Gulati and N. Shankaraiah, *Org. Chem. Front.*, 2021, **8**, 4237–4287.
91 C. G. Neochoritis, T. Zhao and A. Dömling, *Chem. Rev.*, 2019, **119**, 1970–2042.
92 A. C. Boukis, K. Reiter, M. Frölich, D. Hofheinz and M. A. Meier, *Nat. Commun.*, 2018, **9**, 1–10.
93 R. Mittal and S. K. Awasthi, *Synthesis*, 2019, **51**, 3765–3783.
94 V. Ostrovskii, E. Popova and R. Trifonov, in *Advances in heterocyclic chemistry*, Elsevier, 2017, vol. 123, pp. 1–62.
95 A. Singh and R. Kumar, *Chem. Commun.*, 2021, **57**, 9708–9711.
96 R. J. Herr, *Bioorg. Med. Chem.*, 2002, **10**, 3379–3393.
97 L. V. Myznikov, S. V. Vorona and Y. E. Zevatskii, *Chem. Heterocycl. Compd.*, 2021, **57**, 224–233.
98 E. A. Popova, R. E. Trifonov and V. A. Ostrovskii, *Russ. Chem. Rev.*, 2019, **88**, 644.
99 N. R. Penthala, S. Bommagani, J. Yadlapalli and P. A. Crooks, *Tetrahedron Lett.*, 2016, **57**, 1807–1810.
100 N. Kaushik, N. Kumar, A. Kumar and U. K. Singh, *Immunol., Endocr. Metab. Agents Med. Chem.*, 2018, **18**, 3–21.
101 N. M. Aljamali, R. M. U. Mahmood and R. A. Baqi, *Int. J. Anal. Appl. Chem.*, 2020, **6**, 50–60.
102 A. Nguyen, E. Dallerba and A. B. Lowe, *Macromol. Rapid Commun.*, 2022, 2200096.
103 J. H. Mohammed, *Eur. Acad. Res.*, 2016, **3**, 12803.
104 M. Asif, *Pharm. Methods*, 2014, **5**, 39–46.
105 P. Mohite and V. Bhaskar, *J. Optoelectron. Biomed. Mater.*, 2011, **3**, 87–93.
106 V. Ostrovskii, R. Trifonov and E. Popova, *Russ. Chem. Bull.*, 2012, **61**, 768–780.
107 L. Li, T. Wang, Z. Xu, W. Zhou and X.-F. Yu, *Nanoscale*, 2022, **14**, 3929–3934.
108 S. Song, T. Yang, R. Shi and Q. Li, *RSC Adv.*, 2021, **11**, 711–720.
109 S. Swami, S. N. Sahu and R. Shrivastava, *RSC Adv.*, 2021, **11**, 39058–39086.

110 H. Tourani, M. R. Naimi-Jamal and M. G. Dekamin, *ChemistrySelect*, 2018, **3**, 8332–8337.
111 U. Bhatt, *Modern Heterocyclic Chemistry*, 2011, pp. 1401–1430.
112 F. Himo, Z. P. Demko, L. Noodleman and K. B. Sharpless, *J. Am. Chem. Soc.*, 2003, **125**, 9983–9987.
113 S. Zhao, S. Zhang, J. Xu and L. Hu, *Tetrahedron*, 2020, **76**, 131517.
114 F. Matloubi Moghaddam, M. Eslami and N. Ghadirian, *Sci. Iran.*, 2019, **26**, 1463–1473.
115 M. Nikoorazm, P. Moradi and N. Noori, *J. Porous Mater.*, 2020, **27**, 1159–1169.
116 M. Nasrollahzadeh, Y. Bayat, D. Habibi and S. Moshaee, *Tetrahedron Lett.*, 2009, **50**, 4435–4438.
117 M. L. Kantam, K. B. Shiva Kumar and K. Phani Raja, *J. Mol. Catal. A: Chem.*, 2006, **247**, 186–188.
118 R. Shelkar, A. Singh and J. Nagarkar, *Tetrahedron Lett.*, 2013, **54**, 106–109.
119 E. Aali, M. Gholizadeh and N. Noroozi-Shad, *J. Mol. Struct.*, 2022, **1247**, 131289.
120 A. H. Fattahi, M. G. Dekamin and J. H. Clark, *Sci. Rep.*, 2023, **13**, 2803.
121 B. Fattahi and M. G. Dekamin, *Sci. Rep.*, 2023, **13**, 401.
122 M. G. Dekamin, E. Arefi and A. Yaghoubi, *RSC Adv.*, 2016, **6**, 86982–86988.
123 A. Zebardasti, M. G. Dekamin, E. Doustkhah and M. H. N. Assadi, *Inorg. Chem.*, 2020, **59**, 11223–11227.
124 P. Akbarzadeh, N. Koukabi and E. Kolvari, *Res. Chem. Intermed.*, 2019, **45**, 1009–1024.
125 Z. N. Tisseh, M. Dabiri, M. Nobahar, H. R. Khavasi and A. Bazgir, *Tetrahedron*, 2012, **68**, 1769–1773.
126 Z. Hajizadeh, F. Hassanzadeh-Afruzi, D. F. Jelodar, M. R. Ahghari and A. Maleki, *RSC Adv.*, 2020, **10**, 26467–26478.
127 M. Khodamorady and K. Bahrami, *Chemistryselect*, 2019, **4**, 8183–8194.
128 N. Ahmed and Z. N. Siddiqui, *RSC Adv.*, 2015, **5**, 16707–16717.
129 E. Valiey and M. G. Dekamin, *RSC Adv.*, 2022, **12**, 437–450.
130 A. Nouri Parouch, N. Koukabi and E. Abdous, *Res. Chem. Intermed.*, 2020, **46**, 3295–3310.
131 P. Akbarzadeh, N. Koukabi and M. M. Hosseini, *J. Heterocycl. Chem.*, 2020, **57**, 2455–2465.
132 J. Safaei-Ghomi and S. Paymard-Samani, *Chem. Heterocycl. Compd.*, 2015, **50**, 1567–1574.
133 X. Yuan, Z. Wang, Q. Zhang and J. Luo, *RSC Adv.*, 2019, **9**, 23614–23621.
134 C. Behloul, M. Benlahrech, F. Foubelo, C. Nájera and M. Yus, *Synthesis*, 2018, **50**, 3430–3435.
135 B. Chattopadhyay, C. I. R. Vera, S. Chuprakov and V. Gevorgyan, *Org. Lett.*, 2010, **12**, 2166–2169.
136 J. Bonnamour and C. Bolm, *Chem.–Eur. J.*, 2009, **15**, 4543–4545.
137 S. Khaghaninejad, M. M. Heravi, T. Hosseinnejad, H. A. Oskooie and M. Bakavoli, *Res. Chem. Intermed.*, 2016, **42**, 1593–1610.